

Linear Matrix Inequalities for Rigid-Body Inertia Parameter Identification: A Statistical Perspective

Patrick M. Wensing, Sangbae Kim, Jean-Jacques E. Slotine

Abstract—With the increased application of model-based whole-body control methods in legged robots, there has been an resurgence of interest in system identification strategies and adaptive control. An important class of methods relates to the identification of *inertia parameters* for rigid-body systems. For each link, these consist of the mass, first mass moment (related to center of mass location), and 3D rotational inertia tensor. The main contribution of this paper is to formulate physical-consistency constraints on these parameters as Linear Matrix Inequalities (LMIs). Matrix inequalities are found not in terms of moments of inertia, but in terms of statistical moments, suggesting a statistical perspective on the mass distribution of a rigid body. Through this viewpoint, a rich set of new constraints can be formulated as LMIs that enforce properties on the underlying mass distribution of each link. Overall, new constraints have a simpler form, are more efficient to enforce in optimization, and are tighter than those used in the current literature. The methods are verified in system identification for a leg of the MIT Cheetah 3 robot. Detailed properties of transmission components are identified alongside link inertias, with parameter optimization carried out to guaranteed global optimality through semidefinite programming.

I. INTRODUCTION

Recent advances in whole-body control of humanoid and quadruped robots alike have led to a rebirth of model-based control approaches in recent years [1], [2], [3], [4], [5] with many successful demonstrations in large-scale robotic platforms [6], [7], [8], [9]. These diverse methods commonly employ optimization, either explicitly or implicitly through pseudoinverse techniques, over the actuator torques to impart desired characteristics of motion to the robot. Recent strides in torque-controlled actuation have provided wide benefit to whole-body control techniques, while yet emerging actuator designs for legged machines [10] suggest that the performance of these methodologies will continue to improve.

Yet, the performance of whole-body control techniques is heavily dependent on the accuracy of the dynamic models on which they are based. This has led to a resurgence of activity towards methods for accurate system identification [11], [12], [13], [14], [15]. An important class of model identification problems pertains to the inertia parameters of rigid-body systems [16]. Identification is often pursued offline, however, the mathematics of offline identification have close connections to online adaptive control [17].

A number of recent studies in identification and adaptation have focused on issues relating to the float-base structure of legged systems. Pucci et. al [13] extended the methods

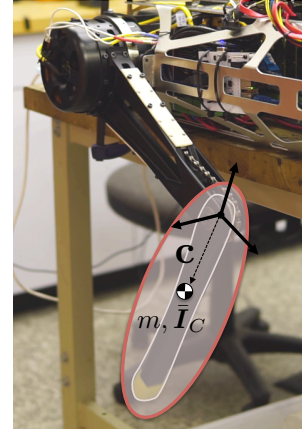


Fig. 1. Experimental setup for system identification on a leg of the MIT Cheetah 3 robot. This work provides new methods to identify masses m , center of mass locations \mathbf{c} , and rotational inertias \mathbf{I}_C of rigid-body systems while ensuring the quantities are physically realizable through a mass distribution within a bounding ellipsoid, depicted in red. Inertia parameters are identified alongside transmission components through convex optimization.

of Slotine and Li [17] to the case of adaptive control in underactuated systems. Their collocated adaptive control approach guarantees tracking locally on the actuated degrees of freedom while learning inertia parameters. Other work has focused more so on parameter identification issues related to the floating base. Ayusawa et. al [11], [18] demonstrated that full-body inertia parameters can be estimated from contact forces and system kinematics, without measuring joint torques, due to properties of the floating-base dynamics.

Other work has concentrated on enforcing the physical realizability of inertia parameters during identification. Sousa and Cortesão [12] show how positive definite conditions on each body's rotational inertia at the CoM can be formulated as an LMI over unknown inertial parameters. Jovic et. al [15] describe a number of practical constraints to improve the performance of [11], for instance, enforcing the CoM to reside within a bounding box from CAD. Recently, Traversaro et. al [14] described additional conditions for physical realizability of inertia parameters that have been neglected in previous work. The conditions tightly characterize the sets of inertia parameters that can be realized by some physical rigid body. At the expense of this tightness, their constraints required a sequence of nonlinear programs to perform parameter optimization over cleverly chosen manifolds.

The main contribution of this paper is to show how extended physical-realizability conditions for the inertia parameters can be formulated as LMIs. First, it is shown that conditions on the so-called triangle inequalities of inertia [14]

Patrick Wensing, Sangbae Kim, and Jean-Jacques Slotine are with the Department of Mechanical Engineering, Massachusetts Institute of Technology, Cambridge, MA 02140, U.S.A., email:{pwensing, sangbae, jjs}@mit.edu

	Handles Tri. Ineqs.	Convex	Discrete Approx.	Uses LMIs
Sousa <i>et. al</i> [12]		✓	No	✓
Traversaro <i>et. al</i> [14]	✓		No	
Ayusawa <i>et. al</i> [18]	✓	✓	Yes	
This Paper	✓	✓	No	✓

TABLE I

COMPARISON OF FEATURES AMONGST PARAMETER IDENTIFICATION
OPTIMIZATION PROBLEMS FORMULATED IN THE LITERATURE.

can be efficiently formulated as an LMI, while improving on the computational performance of [12]. The LMI is found to match the form of a 4×4 pseudo-inertia matrix appearing in early robotics literature [19]. The matrix, however, can be interpreted as a matrix of statistical moments, suggesting that constraints in inertia parameter identification may be more directly viewed through a perspective of statistics than one of mechanics. With this perspective, results from the statistical problem of moments [20] are translated to enforce new bounding-ellipsoid constraints within parameter identification. Throughout, a statistical interpretation of the mass distribution yields richer constraints on the inertia parameters which are tighter than those in earlier work. Perhaps surprisingly, these constraints also of a simpler form, and are more efficient to enforce in numerical optimization.

The paper is laid out as follows. Section II provides preliminaries regarding rigid-body dynamics and linear matrix inequalities. Section III reviews technical details from [12] and [14], with a high-level comparison in Table I. Section IV presents motivation for the statistical perspective on the mass distribution, culminating in the (re)introduction of the pseudo-inertia matrix. Section V draws on connections with the statistical problem of moments to introduce new characterizations of density realizability with bounding volume constraints. An experimental validation of this approach is provided in Section VI for identification of a leg from the MIT Cheetah 3, shown in Fig. 1. Section VII provides concluding remarks.

II. PRELIMINARIES

A. Notation and Definitions

Throughout the text, the set of real and natural numbers are denoted by \mathbb{R} and \mathbb{N} respectively. \mathbb{R}_+ represents the set of non-negative reals, while \mathbb{R}^n represents the set of $n \times 1$ column vectors with real-valued entries. Similarly $\mathbb{R}^{m \times n}$ represents the set of all $m \times n$ matrices. Unless otherwise specified, scalars and scalar-valued quantities are denoted with italics (a, b, c, \dots) while vectors and vector-valued functions are denoted with upright bold characters ($\mathbf{a}, \mathbf{b}, \mathbf{c}, \dots$). Matrix quantities are denoted with upright bold capitals ($\mathbf{A}, \mathbf{B}, \dots$). $\mathbf{1}_n$ indicates the $n \times n$ identity.

The Special Orthogonal group of rotation matrices is denoted as $\text{SO}(3) = \{\mathbf{R} \in \mathbb{R}^{3 \times 3} : \mathbf{R}^\top \mathbf{R} = \mathbf{1}_3\}$, with its Lie algebra, the set of 3×3 skew-symmetric matrices, denoted $\text{so}(3)$. The Special Euclidean group $\text{SE}(3)$ of homogenous transformations is given by

$$\text{SE}(3) = \left\{ \begin{bmatrix} \mathbf{R} & \mathbf{p} \\ \mathbf{0} & 1 \end{bmatrix} : \mathbf{R} \in \text{SO}(3), \mathbf{p} \in \mathbb{R}^3 \right\}$$

with its Lie algebra $\text{se}(3)$. The set of symmetric matrices in $\mathbb{R}^{n \times n}$ is denoted \mathbb{S}^n , with \mathbb{S}_+^n the positive semidefinite cone, and \mathbb{S}_{++}^n the positive definite cone [21]. The shorthand $\mathbf{A} \succeq \mathbf{B}$ is used to denote $\mathbf{A} - \mathbf{B} \in \mathbb{S}_+^n$ for some $n \in \mathbb{N}$. $\mathbf{A} \succ \mathbf{B}$ similarly denotes $\mathbf{A} - \mathbf{B} \in \mathbb{S}_{++}^n$.

Definition 1 (LMI Representable). *A set $\mathcal{S} \subset \mathbb{R}^n$ is called linear matrix inequality (LMI) representable if there exists $m \in \mathbb{N}$ and constant matrices $\{\mathbf{A}_i\}_{i=0}^m \in \mathbb{S}^m$ such that*

$$\mathcal{S} = \{\mathbf{x} \in \mathbb{R}^n : \mathbf{A}_0 + x_1 \mathbf{A}_1 + \dots + x_n \mathbf{A}_n \succeq \mathbf{0}\}$$

A set is called strictly LMI representable when the inequality can be tightened to hold strictly.

A set that is LMI representable is convex, however the converse is not always true. Thus, LMI representability is a stronger condition than convexity. A set \mathcal{S} being LMI representable has favorable implications for numerical optimization, as constraints $\mathbf{x} \in \mathcal{S}$ can be handled using efficient semidefinite programming techniques [21].

B. Rigid-Body Dynamics

The treatment of rigid-body dynamics here relies heavily on 6D spatial notation [22], [23]. Spatial notation can be one-to-one translated to a corresponding Lie-theoretic notation [24]. A recent technical report nicely describes notational and conceptual correspondences [25].

The dynamics of a rigid-body system can be described by

$$\mathbf{H}(\mathbf{q}) \dot{\boldsymbol{\nu}} + \mathbf{C}(\mathbf{q}, \boldsymbol{\nu}) \boldsymbol{\nu} + \mathbf{g}(\mathbf{q}) = \boldsymbol{\tau} \quad (1)$$

where $\mathbf{H} \in \mathbb{R}^{n_d \times n_d}$ the mass matrix, $n_d \in \mathbb{N}_+$ the number of degrees of freedom, $\mathbf{q} \in \mathcal{Q}$ the configuration with \mathcal{Q} the configuration manifold, $\boldsymbol{\nu} \in \mathbb{R}^{n_d}$ the generalized velocity, $\mathbf{C} \boldsymbol{\nu} \in \mathbb{R}^{n_d}$ and $\mathbf{g} \in \mathbb{R}^{n_d}$ the Coriolis and gravity forces, and $\boldsymbol{\tau} \in \mathbb{R}^{n_d}$ the generalized force. For legged systems, the generalized force $\boldsymbol{\tau}$ has contributions from $n_j \in \mathbb{N}_+$ joint actuator torques $\boldsymbol{\tau}_j \in \mathbb{R}^{n_j}$ and $n_c \in \mathbb{N}$ external contact wrenches $\{\mathbf{f}_{c_k}\}_{k=1}^{n_c} \subset \mathbb{R}^6$ according to

$$\boldsymbol{\tau} = \mathbf{S}_j^\top \boldsymbol{\tau}_j + \sum_{k=1}^{n_c} \mathbf{J}_{c_k}^\top \mathbf{f}_{c_k}$$

where $\mathbf{S}_j \in \mathbb{R}^{n_j \times n_d}$ is an actuated joint selector matrix and $\mathbf{J}_{c_k} \in \mathbb{R}^{6 \times n_d}$ the 6D Jacobian for contact k .

The equations (1) can be derived using a Kaneian approach [26] which is effectively employed in standard Recursive Newton-Euler algorithms [23]. Suppose a system of $n_b \in \mathbb{N}_+$ bodies, with coordinate systems attached rigidly to each body. The spatial (6D) velocity $\mathbf{v}_i \in \mathbb{R}^6$ of each body can be described by

$$\mathbf{v}_i(\mathbf{q}, \boldsymbol{\nu}) = \begin{bmatrix} \boldsymbol{\omega}_i \\ \mathbf{v}_i \end{bmatrix} = \mathbf{J}_i(\mathbf{q}) \boldsymbol{\nu} \quad (2)$$

where $\mathbf{J}_i \in \mathbb{R}^{6 \times n_d}$ the Jacobian for body i , $\boldsymbol{\omega}_i \in \mathbb{R}^3$ the angular velocity in body coordinates, and $\mathbf{v}_i \in \mathbb{R}^3$ the linear velocity of the coordinate origin (given in body coordinates). The spatial acceleration $\mathbf{a}_i \in \mathbb{R}^6$ of each body is then

$$\mathbf{a}_i(\mathbf{q}, \boldsymbol{\nu}, \dot{\boldsymbol{\nu}}) = \dot{\mathbf{v}}_i = \dot{\mathbf{J}}_i \boldsymbol{\nu} + \mathbf{J}_i \dot{\boldsymbol{\nu}} \quad (3)$$

The Newton-Euler equations for a rigid body follow [23]:

$$\mathbf{f}_i = \mathbf{I}_i \mathbf{a}_i + (\mathbf{v}_i \times^*) \mathbf{I}_i \mathbf{v}_i \quad (4)$$

where $\mathbf{f}_i \in \mathbb{R}^6$ the net wrench on body i , and $(\mathbf{v}_i \times^*) \in \mathbb{R}^{6 \times 6}$ the spatial cross product matrix [22] for \mathbf{v}_i . The body spatial inertia $\mathbf{I}_i \in \mathbb{R}^{6 \times 6}$ is a constant quantity and is given by

$$\mathbf{I}_i = \begin{bmatrix} \bar{\mathbf{I}}_i & m_i \mathbf{S}(\mathbf{c}_i) \\ m_i \mathbf{S}(\mathbf{c}_i)^\top & m_i \mathbf{1}_3 \end{bmatrix}$$

with $\mathbf{S}(\mathbf{x}) \in \text{so}(3)$ the skew-symmetric matrix such that $\mathbf{S}(\mathbf{x})\mathbf{y} = \mathbf{x} \times \mathbf{y}$ for all $\mathbf{x}, \mathbf{y} \in \mathbb{R}^3$, $\mathbf{c}_i \in \mathbb{R}^3$ the CoM of body i in local coordinates, $m_i \in \mathbb{R}_+$ the body mass, and $\bar{\mathbf{I}}_i \in \mathbb{S}_{++}^3$ a standard 3D rotational inertia tensor about the coordinate origin. The body dynamics can account for the effects of gravity by noting that $\mathbf{f}_i = \mathbf{f}_i^e + \mathbf{I}_i^i \mathbf{a}_g$ where $\mathbf{f}_i^e \in \mathbb{R}^6$ is the gravitational acceleration in frame i and \mathbf{f}_i^e represents the net external wrench on body i (from actuators or other external forces). Finally, (1) is formed by projecting all external wrenches back to generalized forces [26]

$$\begin{aligned} \sum_{i=1}^{n_b} \mathbf{J}_i^\top \mathbf{f}_i^e &= \mathbf{H}(\mathbf{q}) \dot{\boldsymbol{\nu}} + \mathbf{C}(\mathbf{q}, \boldsymbol{\nu}) \boldsymbol{\nu} + \mathbf{g}(\mathbf{q}) \\ &= \sum_{i=1}^{n_b} \mathbf{J}_i^\top (\mathbf{I}_i \mathbf{a}_i - \mathbf{I}_i^i \mathbf{a}_g + (\mathbf{v}_i \times^*) \mathbf{I}_i \mathbf{v}_i) \end{aligned} \quad (5)$$

C. Inertia Parameter Effects on the Equations of Motion

The equations of motion (1) can be described linearly for a specific parameterization of each \mathbf{I}_i [16]. Letting

$$\bar{\mathbf{I}}_i = \begin{bmatrix} I_{xx} & I_{xy} & I_{xz} \\ I_{xy} & I_{yy} & I_{yz} \\ I_{xz} & I_{yz} & I_{zz} \end{bmatrix}$$

and $\mathbf{h}_i = [h_x, h_y, h_z]^\top = m_i \mathbf{c}_i$, it follows that both the spatial inertia \mathbf{I}_i and the net wrench \mathbf{f}_i in (4) can be expressed linearly in the *body inertia parameters* $\boldsymbol{\pi}_i$

$$\boldsymbol{\pi}_i = [m, h_x, h_y, h_z, I_{xx}, I_{xy}, I_{xz}, I_{yy}, I_{yz}, I_{zz}]^\top \in \mathbb{R}^{10}$$

Let $\pi_{ik} \in \mathbb{R}$ denote the k -th parameter for body i , with \mathbf{I}_k the fixed basis such that $\mathbf{I}(\boldsymbol{\pi}_i) = \sum_k \mathbf{I}_k \pi_{ik}$. Parameters for all bodies are collected as

$$\boldsymbol{\pi} = [\boldsymbol{\pi}_1^\top, \dots, \boldsymbol{\pi}_{n_b}^\top]^\top$$

Expanding the role of each π_{ik} in (5)

$$\boldsymbol{\tau} = \sum_{(i,k)} \mathbf{J}_i^\top (\mathbf{I}_k \mathbf{a}_i - \mathbf{I}_k^i \mathbf{a}_g + (\mathbf{v}_i \times^*) \mathbf{I}_k \mathbf{v}_i) \pi_{ik} \quad (6)$$

Combining (6) with (2) and (3) it follows that a regressor matrix $\mathbf{Y} \in \mathbb{R}^{n_j \times 10n_b}$ [17] can be constructed such that

$$\boldsymbol{\tau} = \mathbf{Y}(\mathbf{q}, \boldsymbol{\nu}, \dot{\boldsymbol{\nu}}) \boldsymbol{\pi} \quad (7)$$

The regressor matrix provides a simple method to pursue inertia parameter identification. Given $n_s \in \mathbb{N}_+$ samples $\{\mathbf{q}^{(m)}, \boldsymbol{\nu}^{(m)}, \dot{\boldsymbol{\nu}}^{(m)}, \boldsymbol{\tau}^{(m)}\}_{m=1}^{n_s}$ a simple least squares parameter identification problem can be formulated as [12]

$$\min_{\boldsymbol{\pi}} \sum_m \|\mathbf{Y}^{(m)} \boldsymbol{\pi} - \boldsymbol{\tau}^{(m)}\|^2 \quad (8)$$

This optimization problem is efficiently solvable to global optimality. However, without including constraints, the 6D inertias $\mathbf{I}(\boldsymbol{\pi}_i)$ may not correspond to any physical system.

Inertia parameters in any physical body are determined by its distribution of density $\rho_i(\cdot) : \mathbb{R}^3 \rightarrow \mathbb{R}_+$. The inertia components for each body i are a functional of $\rho_i(\cdot)$ [14]

$$m_i = \iiint_{\mathbb{R}^3} \rho_i(\mathbf{x}) d\mathbf{x} \quad (9)$$

$$m_i \mathbf{c}_i = \iiint_{\mathbb{R}^3} \mathbf{x} \rho_i(\mathbf{x}) d\mathbf{x} \quad (10)$$

$$\bar{\mathbf{I}}_i = \iiint_{\mathbb{R}^3} \mathbf{S}(\mathbf{x}) \mathbf{S}(\mathbf{x})^\top \rho_i(\mathbf{x}) d\mathbf{x} \quad (11)$$

Definition 2 (Density Realizable). *Given a set $\mathcal{X} \subseteq \mathbb{R}^3$, an inertia tensor \mathbf{I} is called \mathcal{X} -density realizable if $\exists \rho(\cdot) : \mathbb{R}^3 \rightarrow \mathbb{R}_+$ such that $\rho(\mathbf{x}) = 0$ if $\mathbf{x} \notin \mathcal{X}$ and the components of \mathbf{I} , $(m, m\mathbf{c}, \bar{\mathbf{I}})$, satisfy (9)-(11) respectively. When \mathcal{X} is not specified, $\mathcal{X} = \mathbb{R}^3$ is assumed.*

Remark 1. *Given any $\mathcal{X} \subseteq \mathbb{R}^3$, the set $\mathcal{P}_{\mathcal{X}}^*$ defined by $\mathcal{P}_{\mathcal{X}}^* = \{\boldsymbol{\pi} \in \mathbb{R}^{10} : m(\boldsymbol{\pi}) > 0, \mathbf{I}(\boldsymbol{\pi}) \text{ is } \mathcal{X}\text{-density realizable}\}$ is a convex cone. This follows from the fact that (9)-(11) are linear in $\rho(\cdot)$. Previous work [18] provided a discrete approximation to this cone. Without discretizing, the work here provides cases wherein this cone is LMI representable.*

III. PREVIOUS RESULTS

This section focuses on physical consistency for a single rigid body. As such, body indices will be dropped. Attempts to enforce physical consistency focus on the rotational inertia $\bar{\mathbf{I}}_C$ about the CoM. The parallel axis theorem in 3D establishes a correspondence between $\bar{\mathbf{I}}_C$ and $\bar{\mathbf{I}}$, the rotational inertia about the local coordinate origin, through

$$\bar{\mathbf{I}} = \bar{\mathbf{I}}_C + m \mathbf{S}(\mathbf{c}) \mathbf{S}(\mathbf{c})^\top \quad (12)$$

A. Physical Semi-consistency: An LMI Parameterization

Positive definite constraints on $\bar{\mathbf{I}}_C(\boldsymbol{\pi})$ have been enforced commonly for the inertia parameters $\boldsymbol{\pi}$ [12], [27]. In a rigid-body system, when each $m_i > 0$ and $\bar{\mathbf{I}}_{C_i} \succ 0$, it can be shown that $\mathbf{H}(\mathbf{q}) \succ 0 \forall \mathbf{q} \in \mathcal{Q}$ [27]. In the case of adaptive control, satisfaction of this constraint on $\mathbf{H}(\mathbf{q})$ throughout adaptation is sufficient to admit tracking guarantees [27]. However, as detailed in [14], $\bar{\mathbf{I}}_C(\boldsymbol{\pi}) \succ 0$ is not sufficient for density realizability of $\mathbf{I}(\boldsymbol{\pi})$.

Definition 3 (Physical Semi-consistency). *A vector of inertia parameters $\boldsymbol{\pi} \in \mathbb{R}^{10}$ is called physically semi-consistent if $m(\boldsymbol{\pi}) > 0$ and $\bar{\mathbf{I}}_C(\boldsymbol{\pi}) \succ 0$. The set of physically semi-consistent parameters is denoted $\mathcal{P} \subset \mathbb{R}^{10}$.*

Theorem 1 (LMI Representation of \mathcal{P}). *[12] The set of physically semi-consistent parameters \mathcal{P} is strictly LMI representable. Its LMI representation is given as*

$$\mathcal{P} = \{\boldsymbol{\pi} \in \mathbb{R}^{10} : \mathbf{I}(\boldsymbol{\pi}) \succ 0\}$$

Extending the optimization of (8) to include physical semi-consistency constraints results in a semidefinite programming (SDP) problem, which can be solved to global

optimality with SDP solvers [21]

$$\begin{aligned} \min_{\boldsymbol{\pi}} \quad & \sum_m \|\mathbf{Y}^{(m)} \boldsymbol{\pi} - \boldsymbol{\tau}^{(m)}\|^2 \\ \text{s.t.} \quad & \mathbf{I}(\boldsymbol{\pi}_i) \succ 0 \quad \forall i \in \{1, \dots, n_b\} \end{aligned}$$

B. (Full) Physical Consistency: Nonlinear Parameterization

Definition 4 (Physical Consistency). *A vector of inertia parameters $\boldsymbol{\pi} \in \mathbb{R}^{10}$ is called physically consistent if*

$$m(\boldsymbol{\pi}) > 0 \text{ and } \mathbf{I}(\boldsymbol{\pi}) \text{ is density realizable.}$$

The set of physically consistent parameters is denoted \mathcal{P}^ .*

In comparison to \mathcal{P} , the set of physically consistent inertia parameters $\mathcal{P}^* \subset \mathcal{P}$ has been shown to result from only three additional conditions on $\bar{\mathbf{I}}_C$ [14]. These additional constraints arise from considerations regarding the principal moments of inertia. Suppose $\mathbf{R} \in \text{SO}(3)$ and $\mathbf{J} = \text{diag}(J_1, J_2, J_3)$, $J_1, \dots, J_3 > 0$ such that $\bar{\mathbf{I}}_C = \mathbf{R}\mathbf{J}\mathbf{R}^\top$. Then, the cartesian inertia tensor is density realizable iff

$$J_1 + J_2 \geq J_3, \quad J_2 + J_3 \geq J_1, \quad \text{and} \quad J_1 + J_3 \geq J_2 \quad (13)$$

Definition 5 (Triangle Inequalities). *A matrix in \mathbb{S}^3 is said to satisfy the triangle inequalities if its eigenvalues $\{J_i\}_{i=1}^3$ satisfy (13).*

Theorem 2 (Nonlinear Parameterization of \mathcal{P}^*). *[14] An inertia tensor \mathbf{I} is physically consistent if and only if there exists $m > 0$, $\mathbf{R} \in \text{SO}(3)$, $\mathbf{J} = \text{diag}(J_1, J_2, J_3) \succ 0$ which satisfies the triangle inequalities, and $\mathbf{c} \in \mathbb{R}^3$ such that*

$$\mathbf{I} = \begin{bmatrix} \mathbf{R}\mathbf{J}\mathbf{R}^\top + m\mathbf{S}(\mathbf{c})\mathbf{S}(\mathbf{c})^\top & m\mathbf{S}(\mathbf{c}) \\ m\mathbf{S}(\mathbf{c})^\top & m\mathbf{1}_3 \end{bmatrix}$$

Even for a single rigid body, optimization with this parameterization of \mathcal{P}^* results is a nonlinear optimization problem over a manifold

$$\begin{aligned} \min_{\mathbf{R}, \mathbf{J}, \mathbf{c}, m} \quad & \sum_m \|\mathbf{Y}^{(m)} \boldsymbol{\pi}(\mathbf{R}, \mathbf{J}, \mathbf{c}, m) - \boldsymbol{\tau}^{(m)}\|^2 \\ \text{s.t.} \quad & \mathbf{R} \in \text{SO}(3) \\ & m > 0, \quad J_i > 0, i = 1, 2, 3 \\ & J_1 + J_2 \geq J_3, \quad J_2 + J_3 \geq J_1, \quad \text{and} \quad J_1 + J_3 \geq J_2 \end{aligned}$$

Solution of this problem is possible using novel methods in [14]. However, the optimization approach requires custom solvers and does not guarantee global optimality.

IV. CONTRIBUTION: AN LMI FOR PHYSICALLY CONSISTENT INERTIA PARAMETERS

This section takes a closer look at the conditions which are required for physical consistency. It is shown that, in fact, the triangle inequalities can be expressed directly as an LMI on the traditional parameters $\boldsymbol{\pi}$, without resorting to an explicit parametrization of $\bar{\mathbf{I}}_C$. Section IV-A first describes a matrix inequality that captures the triangle inequalities on $\bar{\mathbf{I}}_C$. A physical interpretation on this matrix inequality is given in Section IV-B through the introduction of the *density-weighted covariance* of a rigid body and its standard-deviation ellipsoid. Following this interpretation, Section IV-C details an LMI directly over $\boldsymbol{\pi}$ for physical consistency.

A. A matrix inequality for triangle inequalities on $\bar{\mathbf{I}}_C$

Suppose \mathbf{R} and \mathbf{J} as before such that $\bar{\mathbf{I}}_C = \mathbf{R}\mathbf{J}\mathbf{R}^\top$. The triangle inequalities on $\bar{\mathbf{I}}_C$ (13) can be rewritten as

$$J_1 + J_2 + J_3 \geq 2J_i \quad (14)$$

for each $i = 1, \dots, 3$. Noting that J_1, \dots, J_3 are the eigenvalues of $\bar{\mathbf{I}}_C$, (14) is equivalent to

$$\text{Tr}(\bar{\mathbf{I}}_C) \geq 2\lambda_{\max}(\bar{\mathbf{I}}_C) \quad (15)$$

where $\lambda_{\max}(\cdot)$ provides the maximum eigenvalue of its argument, and $\text{Tr}(\cdot)$ is the trace operator. From the eigenvalue inequality $\lambda_{\max}(\bar{\mathbf{I}}_C) \mathbf{x}^\top \mathbf{x} \geq \mathbf{x}^\top \bar{\mathbf{I}}_C \mathbf{x}$, it follows that

$$\lambda_{\max}(\bar{\mathbf{I}}_C) \mathbf{1}_3 \succeq \bar{\mathbf{I}}_C \quad (16)$$

Thus, through the use of (16), (15) is LMI equivalent to

$$\frac{1}{2} \text{Tr}(\bar{\mathbf{I}}_C) \mathbf{1}_3 - \bar{\mathbf{I}}_C \succeq 0 \quad (17)$$

B. The Density-Weighted Covariance of a Rigid Body

The mathematical condition in (17) can be interpreted more cleanly as requiring a positive semidefinite covariance of the rigid body in a density-weighted sense. Towards this insight, $\bar{\mathbf{I}}_C$ can be expanded algebraically to verify

$$\begin{aligned} \bar{\mathbf{I}}_C &= \iiint_{\mathbb{R}^3} \mathbf{S}(\mathbf{x}_c) \mathbf{S}(\mathbf{x}_c)^\top \rho(\mathbf{x}) d\mathbf{x} \\ &= \iiint_{\mathbb{R}^3} (\text{Tr}(\mathbf{x}_c \mathbf{x}_c^\top) \mathbf{1}_3 - \mathbf{x}_c \mathbf{x}_c^\top) \rho(\mathbf{x}) d\mathbf{x} \end{aligned}$$

where $\mathbf{x}_c = \mathbf{x} - \mathbf{c}$. To simplify this expression, the *density-weighted covariance* of a rigid body is introduced as

$$\boldsymbol{\Sigma}_C = \iiint_{\mathbb{R}^3} \mathbf{x}_c \mathbf{x}_c^\top \rho(\mathbf{x}) d\mathbf{x} \quad (18)$$

From this definition, it follows that

$$\bar{\mathbf{I}}_C = \text{Tr}(\boldsymbol{\Sigma}_C) \mathbf{1}_3 - \boldsymbol{\Sigma}_C, \quad \text{and} \quad (19)$$

$$\boldsymbol{\Sigma}_C = \frac{1}{2} \text{Tr}(\bar{\mathbf{I}}_C) \mathbf{1}_3 - \bar{\mathbf{I}}_C \quad (20)$$

using $\text{Tr}(\bar{\mathbf{I}}_C) = 2 \text{Tr}(\boldsymbol{\Sigma}_C)$. From (19), it can be seen that $\boldsymbol{\Sigma}_C$ and $\bar{\mathbf{I}}_C$ share a set of eigenvectors. It can further be verified that if μ_1, μ_2, μ_3 the eigenvalues of $\boldsymbol{\Sigma}_C$, then

$$J_1 = \mu_2 + \mu_3, \quad J_2 = \mu_1 + \mu_3, \quad J_3 = \mu_1 + \mu_2 \quad (21)$$

are the eigenvalues of $\bar{\mathbf{I}}_C$. Using these relationships, and in light of (17), the following can be verified.

Proposition 1 (Covariance Interpretation of Triangle Ineqs.). *Suppose $\bar{\mathbf{I}}, \boldsymbol{\Sigma} \in \mathbb{S}^3$, $\boldsymbol{\Sigma} = \frac{1}{2} \text{Tr}(\bar{\mathbf{I}}) \mathbf{1}_3 - \bar{\mathbf{I}}$. Then $\boldsymbol{\Sigma} \succeq 0$ if and only if $\bar{\mathbf{I}} \succeq 0$ and $\bar{\mathbf{I}}$ satisfies the triangle inequalities. An analogous statement holds with all inequalities tightened to hold strictly.*

A similar proposition can be found within [28], however, the physical connection to the density-weighted covariance provided here is new. The following corollary is an immediate result of combining Proposition 1 with (17).

Corollary 1 (Parameterization of \mathcal{P}^* with an LMI on $\boldsymbol{\Sigma}_C$). *$\boldsymbol{\pi} \in \mathcal{P}^*$ if and only if $m(\boldsymbol{\pi}) > 0$ and $\boldsymbol{\Sigma}_C(\boldsymbol{\pi}) \succeq 0$.*

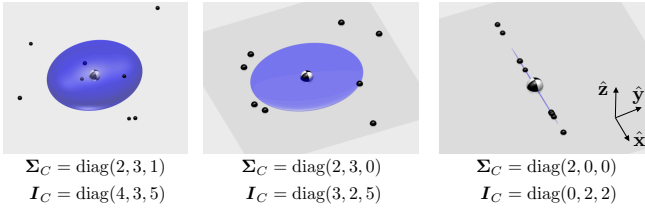


Fig. 2. Graphical representation of Σ_C . Point mass distribution examples when (a) $\Sigma_C \succ 0$ (all triangle inequalities hold strictly) (b) $\Sigma_C \succeq 0$ with one zero eigenvalue, and thus one triangle inequality is tight. (c) $\Sigma_C \succeq 0$ with two zero eigenvalues, and thus two triangle inequalities are tight. The blue ellipsoid is defined as the standard-deviation ellipsoid \mathcal{E}_π in the text, and represents one standard deviation in each direction of its extent.

To help visualize Σ_C , an ellipsoid \mathcal{E}_π is defined as

$$\mathcal{E}_\pi = \{\mathbf{x} \in \mathbb{R}^3 : \exists \mathbf{y}, \Sigma_C \mathbf{y} = (\mathbf{x} - \mathbf{c}), (\mathbf{x} - \mathbf{c})^\top \mathbf{y} = 1\}$$

which, when $\Sigma_C \succ 0$, takes the form

$$\mathcal{E}_\pi = \{\mathbf{x} \in \mathbb{R}^3 : (\mathbf{x} - \mathbf{c})^\top \Sigma_C^{-1} (\mathbf{x} - \mathbf{c}) = 1\}$$

This set is named the *standard-deviation ellipsoid*. In the case of a 1D probability distribution, some of the probability density must exist at or beyond the standard deviation. This intuition generalizes to 3D. At least some of the mass of the body must exist on or beyond the ellipsoidal shell \mathcal{E}_π .

The standard-deviation ellipsoid \mathcal{E}_π is shown in Figure 2 for different density distributions. When Σ_C has a zero eigenvalue, the density distribution is degenerate. An infinitely thin plate, for instance, has no variance normal to the plate, and thus would have a single zero eigenvalue in Σ_C , as in Fig. 2(b). Correspondingly, one of the triangle inequalities holds tightly in such a case. Since any physical body must have non-infinitesimal spatial extent in all directions, it suffices to consider physical realizability under the condition that the triangle inequalities hold with strict inequality.

Remark 2. Corollary 1 can be interpreted cleanly within a probabilistic context. Suppose $\mathbf{X} \in \mathbb{R}^3$ a random variable with $p(\cdot) = \rho(\cdot)/m$ its mass-normalized probability density function. Define $E[\cdot]$ the expectation operation. Corollary 1 effectively states that the covariance of \mathbf{X} , given by $E[(\mathbf{X} - E[\mathbf{X}])(\mathbf{X} - E[\mathbf{X}])^\top]$, is non-degenerate density realizable if and only if the covariance is positive definite. Thus, from the standpoint of statistics, this new condition on density realizability may be rather unsurprising in hindsight.

Remark 3. Corollary 1 could have applicability to inertia identification and adaptive methods within attitude control of aerial vehicles (e.g. [29], [30], [31]). In these applications, the CoM location is often assumed known, and focus is placed on estimating the CoM inertia \bar{I}_C . The triangle inequalities are often overlooked, but are treated in e.g. [32], [33]. Corollary 1 could be considered to address the triangle inequalities within this thread of research.

C. An LMI Representation of Physical Consistency

While (17) and its covariance interpretation provide a matrix inequality for the physical consistency of \bar{I}_C , this condition is not linear in the inertia parameters π . An analog

of the parallel axis theorem for Σ_C , however, will admit an LMI characterization similar to that provided in Theorem 1.

The matrix of second moments $\Sigma \in \mathbb{R}^{3 \times 3}$ is defined as

$$\Sigma = \iiint_{\mathbb{R}^3} \mathbf{x} \mathbf{x}^\top \rho(\mathbf{x}) d\mathbf{x}$$

Through expansion of (18) and using (9) and (10), an analog to the parallel axis theorem can be verified as:

$$\Sigma = \Sigma_C + m \mathbf{c} \mathbf{c}^\top \quad (22)$$

As a key benefit, using the relationship $\Sigma = \frac{1}{2} \text{Tr}(\bar{I}) \mathbf{1}_3 - \bar{I}$ from (20), Σ is verified linear in the inertia parameters π .

Definition 6 (Pseudo-Inertia Matrix). The pseudo-inertia matrix \mathbf{J} for parameters π is defined by

$$\mathbf{J}(\pi) = \begin{bmatrix} \Sigma(\pi) & \mathbf{h}(\pi) \\ \mathbf{h}(\pi)^\top & m(\pi) \end{bmatrix}$$

Theorem 3 (LMI Representation of \mathcal{P}^*). The set of physically consistent parameters \mathcal{P}^* for a single rigid body is strictly LMI representable. Its LMI representation is

$$\mathcal{P}^* = \{\pi \in \mathbb{R}^{10} : \mathbf{J}(\pi) \succ 0\}$$

Proof. By the Schur complement lemma [21, Section A.5.5], $\mathbf{J}(\pi) \succ 0$ if and only if $m(\pi) > 0$ and $\Sigma - \frac{1}{m} \mathbf{h} \mathbf{h}^\top \succ 0$. By application of the parallel axis theorem for second mass-moment matrices (22), and using $\mathbf{h} = m \mathbf{c}$, this is equivalent to $\Sigma_C \succ 0$. From Proposition 1, this is equivalent to $\bar{I}_C \succ 0$ and \bar{I}_C satisfies the triangle inequalities. Finally, from the main result of [14], this is equivalent to $\pi \in \mathcal{P}^*$. \square

Remark 4. Again, taking a statistical view on the mass distribution of a rigid body, the results of Thm. 3 can be seen to flow from a condition on the statistical first and second moments [34, Thm. 16.1.2]. Suppose $\mu \in \mathbb{R}^3$ and $\mathbf{E} \in \mathbb{S}_+^3$, then there exists a random variable $\mathbf{X} \in \mathbb{R}^3$ such that $\mu = E[\mathbf{X}]$ and $\mathbf{E} = E[\mathbf{X} \mathbf{X}^\top]$ if and only if

$$\begin{bmatrix} \mathbf{E} & \mu \\ \mu^\top & 1 \end{bmatrix} \succeq 0$$

In comparison, the constraint $\mathbf{J}(\pi) \succ 0$ in Thm. 3 multiplies each of these components by the overall mass $m(\pi)$ and enforces non-degeneracy of the distribution.

The 4×4 matrix of moments $\mathbf{J}(\pi)$ was found more commonly in early robot dynamics literature (e.g. [19], [35]) and in early work on adaptive control (e.g. [36]). It has been employed more recently within the context of 4×4 matrix forms of the equations of motion for a rigid body [37], [38]. Using these 4×4 equations, a parameter identification approach for a single rigid body was proposed in [38]. The same matrix $\mathbf{J}(\pi)$ was used to provide a left-invariant Riemannian metric over $\text{SE}(3)$ in [28] and appears in robotics books (e.g. [39]). Despite its importance, the pseudo-inertia matrix is notably lacking from current mainstream literature on robot dynamics.

It is interesting to note how the pseudo inertia $\mathbf{J}(\pi)$ compares to the standard spatial inertia $\mathbf{I}(\pi)$ in terms of the kinetic energy metric each provides. Suppose

$$\mathbf{v} = \begin{bmatrix} \boldsymbol{\omega} \\ \mathbf{v} \end{bmatrix} \in \mathbb{R}^6, \mathbf{V} = \begin{bmatrix} \mathbf{S}(\boldsymbol{\omega}) & \mathbf{v} \\ \mathbf{0} & 0 \end{bmatrix} \in \text{se}(3)$$

It can be verified that the kinetic energy satisfies [39]

$$\frac{1}{2} \mathbf{v}^\top \mathbf{I}(\pi) \mathbf{v} = \frac{1}{2} \text{Tr}(\mathbf{V} \mathbf{J}(\pi) \mathbf{V}^\top)$$

Thus, while physical semi-consistency ensures that the associated kinetic energy metric is positive definite, the additional constraints from the triangle inequalities enforce additional structure on the metric. As has been shown for the first time here, the triangle inequalities are precisely what represent the difference between $\mathbf{I}(\pi) \succ 0$ and $\mathbf{J}(\pi) \succ 0$.

The pseudo-inertia matrix is also of a lower dimension (4×4) than the spatial inertia matrix (6×6). This may be surprising in light of the fact that the 3 additional triangle inequalities are embedded within the LMI for $\mathbf{J}(\pi)$. As a result, however, the LMI $\mathbf{J}(\pi) \succ 0$ is more computationally efficient to enforce than $\mathbf{I}(\pi) \succ 0$.

V. CONTRIBUTION: LMI CONSTRAINTS FOR INERTIA PARAMETER REALIZABILITY ON ELLIPSOIDS

With the statistical perspective of the mass distribution, answering further questions of physical realizability for inertia parameters falls within the body of work on the problem of moments within statistics (e.g. [20], [40]). With this insight, results are translated here to provide new conditions on inertia realizability with bounding volume constraints.

Recent work has shown the benefits of including prior knowledge on the shape of each rigid body within parameter identification. Work by Jovic et. al [15] enforced the CoM to reside within a bounding box estimated from CAD. New constraints are provided here that address second moments.

To begin, suppose a rigid body is known to reside within an ellipsoid $\mathcal{S} \subset \mathbb{R}^3$ described by:

$$\mathcal{S} = \{\mathbf{x} \in \mathbb{R}^3 \mid (\mathbf{x} - \mathbf{x}_s)^\top \mathbf{Q}_s^{-1} (\mathbf{x} - \mathbf{x}_s) \leq 1\} \quad (23)$$

Before considering constraints on the second moments, it is noted that the CoM constraint, $\mathbf{c}(\pi) \in \mathcal{S}$, can be formulated as an LMI over π . When $m(\pi) > 0$, $\mathbf{c}(\pi) \in \mathcal{S}$ iff

$$\mathbf{C}(\pi) = \begin{bmatrix} m(\pi) & \mathbf{h}(\pi)^\top - m(\pi) \mathbf{x}_s^\top \\ \mathbf{h}(\pi) - m(\pi) \mathbf{x}_s & m(\pi) \mathbf{Q}_s \end{bmatrix} \succeq 0 \quad (24)$$

Again, equivalence is due to the Schur complement lemma.

Yet, as the CoM approaches the edge of \mathcal{S} , large second moments would imply the existence of mass outside the ellipsoid. In fact, as the CoM of a rigid body approaches the edge of a bounding ellipsoid, the rigid body necessarily degenerates to a point mass. Thus, constraints that $\mathbf{c}(\pi) \in \mathcal{S}$ alone are not sufficient for π to be \mathcal{S} -density realizable. Drawing on the perspective of statistics, Theorem 4.7(b) from [41] can be translated as follows.

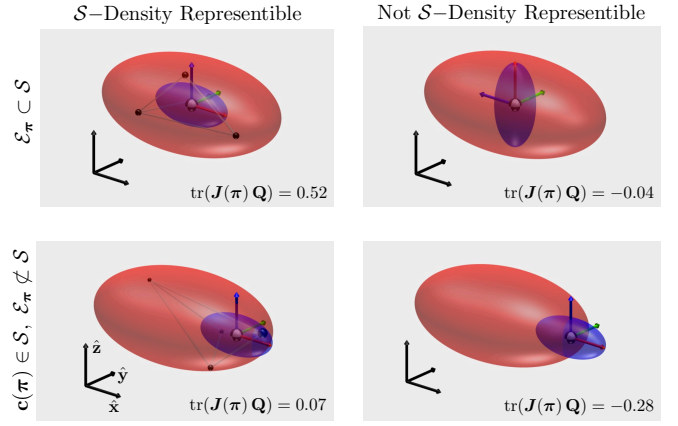


Fig. 3. Cases illustrating the role of the center and shape of the standard-deviation ellipsoid \mathcal{E}_π on \mathcal{S} -density realizability of π . In each case, the ellipsoid \mathcal{S} has semiaxes of length $\sqrt{5}, \sqrt{2}, 1$ in the $\hat{x}, \hat{y}, \hat{z}$ directions. \mathcal{E}_π has semiaxes $\sqrt{0.9}, \sqrt{0.2}, \sqrt{0.2}$ with principle axes colored accordingly in the figure. When a density distribution on \mathcal{S} exists, a distribution by four point masses is shown, as guaranteed to exist through Thm. 4.

Theorem 4 (Density Realizability on an Ellipsoid). *Suppose a bounding ellipsoid \mathcal{S} as in (23). Let $\mathbf{Q} \in \mathbb{R}^{4 \times 4}$ such that*

$$\mathcal{S} = \left\{ \mathbf{x} \in \mathbb{R}^3 : \begin{bmatrix} \mathbf{x} \\ 1 \end{bmatrix}^\top \mathbf{Q} \begin{bmatrix} \mathbf{x} \\ 1 \end{bmatrix} \geq 0 \right\}$$

Then, π is \mathcal{S} -density realizable if and only if

$$\mathbf{J}(\pi) \succ 0 \text{ and } \text{Tr}(\mathbf{J}(\pi) \mathbf{Q}) \geq 0. \quad (25)$$

Further, any π is \mathcal{S} -density realizable iff it can be represented by four point masses m_k at $\mathbf{x}_k \in \mathcal{S}$ such that:

$$\mathbf{J}(\pi) = \sum_{k=1}^4 m_k \begin{bmatrix} \mathbf{x}_k \\ 1 \end{bmatrix} \begin{bmatrix} \mathbf{x}_k \\ 1 \end{bmatrix}^\top$$

Note that by taking into account the second moments, the condition $\text{Tr}(\mathbf{J}(\pi) \mathbf{Q}) \geq 0$ in (25) is a 1D linear inequality constraint, whereas the looser condition (24) is a 4×4 LMI. Thus, again, it is found that the statistical perspective of the mass distribution results in tighter conditions that are computationally more efficient to enforce. Figure 3 shows a number of cases, illustrating both the role of the CoM location and the shape of the standard-deviation ellipsoid \mathcal{E}_π on \mathcal{S} -density realizability. The following corollary is provided to accommodate more complex bounding shapes.

Corollary 2 (Density Realizability on the Union of Ellipses). *Suppose a rigid body is known to reside within the union of n_ℓ ellipses $\mathcal{S} = \cup_{\ell=1}^{n_\ell} \mathcal{S}_\ell$. Then, its inertia parameters π are \mathcal{S} -density realizable if and only if there exist parameters $\{\pi_\ell\}_{\ell=1}^{n_\ell}$ such that $\pi = \sum_{\ell=1}^{n_\ell} \pi_\ell$ and each π_ℓ is \mathcal{S}_ℓ -density realizable as verified by Thm. 4.*

Remark 5. *Beyond identification, LMIs for the sets $\mathcal{P}_\mathcal{S}^* \subset \mathcal{P}_{\mathbb{R}^3}^* \subset \mathcal{P}$ also have applicability for projected gradient methods in adaptive control [42]. In this context, tightening constraints on unknown parameters only increases the rate of parameter convergence [43].*

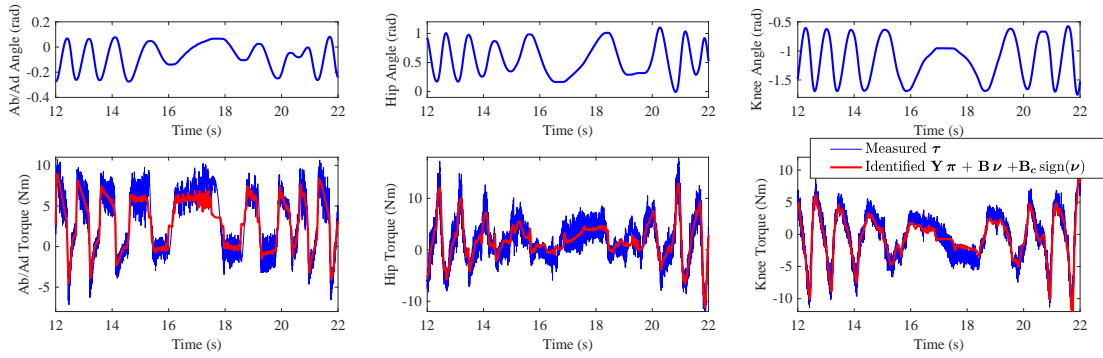


Fig. 4. Regression errors after identification of a leg for the MIT Cheetah 3. The data shown is distinct from that used in training. Motor torques are predicted with an overall RMS error of 1.46 Nm. For comparison, the Coulomb friction was identified as $\mathbf{B}_c = \text{diag}(3.12, 1.25, 0.95)$ Nm.

VI. EXPERIMENTAL VALIDATION

The proposed constraints were used to identify a leg of the MIT Cheetah 3 robot. The robot, shown in Fig. 1, has four 3-DoF legs where each DoF is driven by a proprioceptive actuator [10]. Each actuator includes a large air-gap radius brushless DC motor, with a high-inertia rotor coupled to the joint output by a 11.62 : 1 planetary gearbox. To address the unique characteristics of these actuators, the leg was treated as a system of $n_b = 6$ bodies (3 rigid links, and 3 rotors). Joint rates at the output of the gearbox were used as the generalized velocity ν . To account for transmission losses, (7) was modified via diagonal matrices of viscous and Coulomb friction coefficients $\mathbf{B} \in \mathbb{R}^{3 \times 3}$ and $\mathbf{B}_c \in \mathbb{R}^{3 \times 3}$

$$\tau - \mathbf{B}\nu - \mathbf{B}_c \text{sign}(\nu) = \mathbf{Y}(\mathbf{q}, \nu, \dot{\nu}) \pi \quad (26)$$

Outer approximation bounding-ellipsoid parameters in \mathbf{C}_i and \mathbf{Q}_i were set using geometric properties from CAD.

With the result of Theorem 4, rich physical-consistency constraints on the inertia parameters can be treated while also identifying transmission characteristics.

$$\begin{aligned} \min_{\pi, \mathbf{B}_c, \mathbf{B}} \quad & \frac{1}{n_s} \sum_m \|\mathbf{Y}^{(m)} \pi + \mathbf{B}\nu^{(m)} + \mathbf{B}_c \text{sign}(\nu^{(m)}) - \tau^{(m)}\|^2 \\ & + w_\pi \|\pi - \hat{\pi}\|^2 \\ \text{s.t.} \quad & \mathbf{C}_i(\pi_i) \succeq 0 \quad (\text{CoM within an Ellipse}) \\ & \mathbf{J}(\pi_i) \succ 0 \quad (\text{Density Realizability}) \\ & \text{Tr}(\mathbf{J}(\pi_i) \mathbf{Q}_i) \geq 0 \quad (\text{Density on an Ellipse}) \\ & \forall i \in \{1, \dots, n_b\} \end{aligned} \quad (27)$$

A small regularizing term $w_\pi \|\pi - \hat{\pi}\|^2$ is added where $\hat{\pi} \in \mathbb{R}^{10n_b}$ is a set of estimated inertia parameters from CAD or other sources. Such regularization is common practice [12].

Data was gathered from a leg swinging experiment shown in the supplementary video. To generate the motion, the leg was placed in a Cartesian impedance control mode, and the foot endpoint was commanded to move on a virtual ellipsoidal shell. The target point on the shell was parameterized by spherical angles (ϕ, θ) , governed by rates $\dot{\phi} = A_\phi \sin(\omega_\phi t)$ and $\dot{\theta} = A_\theta \sin(\omega_\theta t)$ with $A_\phi = 12$ rad/s, $A_\theta = 3.4$ rad/s, $\omega_\phi = 1.63$ rad/s, and $\omega_\theta = 0.265$ rad/s. Data was sampled at 1 kHz, with joint actuator torques τ_j estimated from the torques commanded to brushless current controllers [10]. The problem (27) was solved with

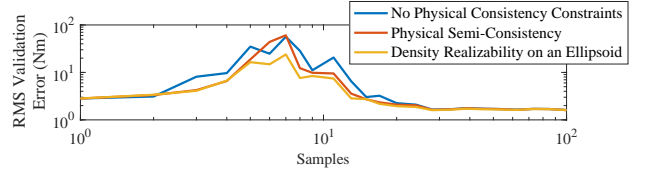


Fig. 5. Validation error after identification versus sample size.

10,000 data samples using CVX [44] and the MOSEK solver [45]. The problem took 1.67s to solve to global optimality on a 2011 Intel Core i5 MacBook Pro. Regularization of $w_\pi = 10^{-6}$ was used.

After identification, the RMS errors from (26) with the next 10,000 samples in the dataset were 1.48, 1.69, and 1.16 Nm on the ab/ad, hip, and knee respectively. For comparison, the Coulomb friction was identified as $\mathbf{B}_c = \text{diag}(3.12, 1.25, 0.95)$ Nm. Figure 4 shows identification results for this validation data. Figure 5 shows how this performance compares for different training sample sizes n_s and with different constraints. As in Remark 5, tighter constraints empirically result in an accurate model more quickly as additional data is used. This benefit is in addition to the fact that tightened constraints result in optimal parameters that are physically realistic.

VII. CONCLUSIONS

This paper has advocated for a statistical perspective of the mass distribution for a rigid body when approaching constraints within inertia parameter identification. Rather than focus on moments of inertia, questions of density realizability are more directly addressed through the density-weighted covariance Σ_C of each body. Through a parallel-axis-like theorem applied to this quantity, results have shown the importance of the pseudo-inertia matrix $\mathbf{J}(\pi)$. This matrix of moments is linear in the inertia parameters, and can be used to efficiently enforce density realizability constraints.

Through the form of $\mathbf{J}(\pi)$, it was argued that constraints on the inertia parameters might instead be viewed as a special case of the problem of moments in statistics. Through this connection, constraints on the density realizability over a bounding ellipsoid, or union of bounding ellipsoids, can be formulated through LMI constraints over the unknown inertia parameters. This result provides a rich set of constraints that can be used to solve physically consistent inertia parameter identification problems to guaranteed global

optimality. Future work will apply the identified models for high-performance control of the MIT Cheetah 3.

ACKNOWLEDGMENT

The authors would like to acknowledge Ben Katz and Jared DiCarlo for assistance with the experiments. Funding for this work was supported in part through NSF award IIS-1350879 and by the Agency for Defense Development of Korea under contract UD140073ID.

REFERENCES

- [1] Y. Abe, M. da Silva, and J. Popović, "Multiobjective control with frictional contacts," in *2007 ACM SIGGRAPH/Eurographics Symp. on Computer Animation*, Aire-la-Ville, Switzerland, 2007, pp. 249–258.
- [2] J. Park, J. Haan, and F. Park, "Convex optimization algorithms for active balancing of humanoid robots," *IEEE Transactions on Robotics*, vol. 23, no. 4, pp. 817–822, Aug. 2007.
- [3] J. Park and O. Khatib, "Contact consistent control framework for humanoid robots," in *Proc. of the IEEE Int. Conference on Robotics and Automation*, May 2006, pp. 1963–1969.
- [4] L. Sentis, J. Park, and O. Khatib, "Compliant control of multicontact and center-of-mass behaviors in humanoid robots," *IEEE Trans. on Robotics*, vol. 26, no. 3, pp. 483–501, June 2010.
- [5] P. M. Wensing and D. E. Orin, "Generation of dynamic humanoid behaviors through task-space control with conic optimization," in *IEEE Int. Conf. on Rob. and Automation*, Karlsruhe, Germany, May 2013, pp. 3103–3109.
- [6] M. Hutter, H. Sommer, C. Gehring, M. Hoepflinger, M. Bloesch, and R. Siegwart, "Quadrupedal locomotion using hierarchical operational space control," *Int. J. of Robotics Research*, vol. 33, no. 8, pp. 1047–1062, 2014.
- [7] J. Koenemann, A. D. Prete, Y. Tassa, E. Todorov, O. Stasse, M. Bennewitz, and N. Mansard, "Whole-body model-predictive control applied to the hrp-2 humanoid," in *IEEE/RSJ International Conference on Intelligent Robots and Systems*, Sept 2015, pp. 3346–3351.
- [8] A. Herzog, N. Rotella, S. Mason, F. Grimmering, S. Schaal, and L. Righetti, "Momentum control with hierarchical inverse dynamics on a torque-controlled humanoid," *Autonomous Robots*, vol. 40, no. 3, pp. 473–491, 2016.
- [9] S. Kuindersma, R. Deits, M. Fallon, A. Valenzuela, H. Dai, F. Permenter, T. Koolen, P. Marion, and R. Tedrake, "Optimization-based locomotion planning, estimation, and control design for the atlas humanoid robot," *Autonomous Robots*, pp. 1–27, 2015.
- [10] P. M. Wensing, A. Wang, S. Seok, D. Otten, J. Lang, and S. Kim, "Proprioceptive actuator design in the MIT cheetah: Impact mitigation and high-bandwidth physical interaction for dynamic legged robots," 2017, *IEEE Transactions on Robotics*.
- [11] K. Ayusawa, G. Venture, and Y. Nakamura, "Identifiability and identification of inertial parameters using the underactuated base-link dynamics for legged multibody systems," *Int. J. of Robotics Research*, vol. 33, no. 3, pp. 446–468, 2014.
- [12] C. D. Sousa and R. Cortesão, "Physical feasibility of robot base inertial parameter identification: A linear matrix inequality approach," *Int. J. of Robotics Research*, vol. 33, no. 6, pp. 931–944, 2014.
- [13] D. Pucci, F. Romano, and F. Nori, "Collocated adaptive control of underactuated mechanical systems," *IEEE Transactions on Robotics*, vol. 31, no. 6, pp. 1527–1536, Dec 2015.
- [14] S. Traversaro, S. Brossette, A. Escande, and F. Nori, "Identification of fully physical consistent inertial parameters using optimization on manifolds," in *IEEE/RSJ Int. Conf. on Intelligent Rob. and Sys.*, Oct 2016, pp. 5446–5451.
- [15] J. Jovic, A. Escande, K. Ayusawa, E. Yoshida, A. Kheddar, and G. Venture, "Humanoid and human inertia parameter identification using hierarchical optimization," *IEEE Transactions on Robotics*, vol. 32, no. 3, pp. 726–735, June 2016.
- [16] C. G. Atkeson, C. H. An, and J. M. Hollerbach, "Estimation of inertial parameters of manipulator loads and links," *The International Journal of Robotics Research*, vol. 5, no. 3, pp. 101–119, 1986.
- [17] J.-J. E. Slotine and W. Li, "On the adaptive control of robot manipulators," *Int. J. of Robotics Research*, vol. 6, no. 3, pp. 49–59, 1987.
- [18] K. Ayusawa, G. Venture, and Y. Nakamura, "Real-time implementation of physically consistent identification of human body segments," in *IEEE Inf. Conf. on Rob. and Auto.*, May 2011, pp. 6282–6287.
- [19] A. K. Bejczy, "Robot arm dynamics and control," JPL Technical Memorandum 33-669, Tech. Rep., 1974.
- [20] J. B. Lasserre, "A semidefinite programming approach to the generalized problem of moments," *Mathematical Programming*, vol. 112, no. 1, pp. 65–92, 2008.
- [21] S. Boyd and L. Vandenberghe, *Convex Optimization*. Cambridge, U.K.: Cambridge Univ. Press, 2004.
- [22] R. Featherstone, *Rigid Body Dynamics Algorithms*. New York, NY: Springer, 2008.
- [23] R. Featherstone and D. Orin, "Chapter 2: Dynamics," in *Springer Handbook of Robotics*, B. Siciliano and O. Khatib, Eds. New York: Springer, 2008.
- [24] F. Park, J. Bobrow, and S. Ploen, "A lie group formulation of robot dynamics," *The International Journal of Robotics Research*, vol. 14, no. 6, pp. 609–618, 1995.
- [25] S. Traversaro and A. Saccon, "Multibody dynamics notation," Technische Universiteit Eindhoven, Tech. Rep., 2016. [Online]. Available: <http://repository.tue.nl/849895>
- [26] T. R. Kane and D. A. Levinson, "The use of Kane's dynamical equations in robotics," *Int. J. of Robotics Research*, vol. 2, no. 3, pp. 3–21, 1983.
- [27] W. Li and J.-J. E. Slotine, "An indirect adaptive robot controller," *Systems & Control Letters*, vol. 12, no. 3, pp. 259 – 266, 1989.
- [28] C. Belta and V. Kumar, "An SVD-based projection method for interpolation on SE(3)," *IEEE Transactions on Robotics and Automation*, vol. 18, no. 3, pp. 334–345, Jun 2002.
- [29] J. Ahmed, V. T. Coppola, and D. S. Bernstein, "Adaptive asymptotic tracking of spacecraft attitude motion with inertia matrix identification," *J. Guid. Control and Dyn.*, vol. 21, no. 5, pp. 684–691, 1998.
- [30] N. A. Chaturvedi, D. S. Bernstein, J. Ahmed, F. Bacconi, and N. H. McClamroch, "Globally convergent adaptive tracking of angular velocity and inertia identification for a 3-dof rigid body," *IEEE Trans. on Control Sys. Technology*, vol. 14, no. 5, pp. 841–853, Sept 2006.
- [31] D. Thakur, S. Srikant, and M. R. Akella, "Adaptive attitude-tracking control of spacecraft with uncertain time-varying inertia parameters," *J. Guidance, Control, and Dynamics*, vol. 38, no. 1, pp. 41–52, 2014.
- [32] M. A. Peck, "Uncertainty models for physically realizable inertia dyadics," *J. Astronautical Sciences*, vol. 54, no. 1, pp. 1–16, 2006.
- [33] Z. Manchester and M. Peck, "Recursive inertia estimation with semidefinite programming," in *AIAA Guidance, Navigation, and Control Conference*, 2017.
- [34] D. Bertsimas and J. Sethuraman, "Moment problems and semidefinite optimization," in *Handbook of Semidefinite Programming*, ser. International Series in Operations Research & Management Science, H. Wolkowicz, R. Saigal, and L. Vandenberghe, Eds. Springer US, 2000, vol. 27, pp. 469–509.
- [35] J. J. Uicker, Jr., "Dynamic force analysis of spatial linkages," *Journal of Applied Mechanics*, vol. 34, no. 2, pp. 418–424, June 1967.
- [36] C. P. Neuman and P. K. Khosla, *Adaptive and Learning Systems*. Springer US, 1986, ch. Identification of Robot Dynamics: An Application of Recursive Estimation, pp. 175–194.
- [37] G. Legnani, F. Casolo, P. Righettini, and B. Zappa, "A homogeneous matrix approach to 3D kinematics and dynamics — I. Theory," *Mechanism and Machine Theory*, vol. 31, no. 5, pp. 573 – 587, 1996.
- [38] E. Atchounglo, C. Vallée, T. Monnet, and D. Fortuné, "Identification of the ten inertia parameters of a rigid body," *Journal of Applied Mathematics and Mechanics*, vol. 72, no. 1, pp. 22 – 25, 2008.
- [39] T. Yoshikawa, *Dynamics*. MIT Press, 2003, pp. 81–126.
- [40] K. Schmudgen, "The K-moment problem for compact semi-algebraic sets," *Mathematische Annalen*, vol. 289, no. 2, pp. 203–206, 1991.
- [41] L. Fialkow and J. Nie, "Positivity of riesz functionals and solutions of quadratic and quartic moment problems," *Journal of Functional Analysis*, vol. 258, no. 1, pp. 328 – 356, 2010.
- [42] J.-J. E. Slotine and J. A. Coetsee, "Adaptive sliding controller synthesis for non-linear systems," *International Journal of Control*, vol. 43, no. 6, pp. 1631–1651, 1986.
- [43] P. A. Ioannou and J. Sun, *Robust adaptive control*. Courier Corporation, 2012.
- [44] M. Grant and S. Boyd, *Cvx: Matlab software for disciplined convex programming*, version 2.0 beta. [Online]. Available: <http://cvxr.com/cvx>
- [45] E. D. Andersen, C. Roos, and T. Terlaky, "On implementing a primal-dual interior-point method for conic quadratic optimization," *Mathematical Programming*, vol. 95, no. 1, pp. 249–277, 2003.